

http://pubs.acs.org/journal/aelccp

Mixed Self-Assembled Monolayers for High-Photovoltage Tin Perovskite Solar Cells

Donghoon Song, Shripathi Ramakrishnan, Yugang Zhang, and Qiuming Yu*



Cite This: ACS Energy Lett. 2024, 9, 1466–1472



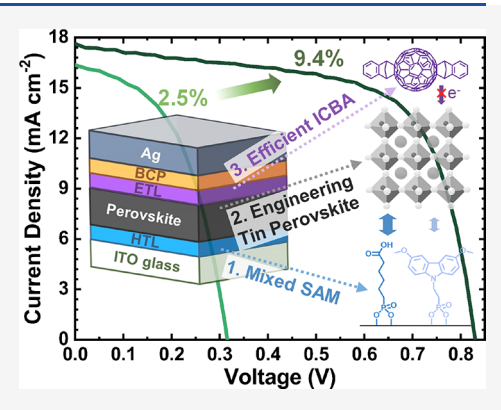
ACCESS I

III Metrics & More

Article Recommendations

Supporting Information

ABSTRACT: Self-assembled monolayers (SAMs) are used as potent hole transport layers (HTLs) in lead-based perovskite solar cells, enabling large quasi-Fermi level splitting for high photovoltage (>1.1 V) with a deficit of <0.5 V. However, tin-based perovskite solar cells (TPSCs) with SAM HTLs suffer from low photovoltage (<0.65 V) with a deficit of >0.7 V. Herein we employ a holistic approach to tackle this significant challenge by designing a mixed SAM, engineering a compatible tin perovskite thin film, and leveraging an efficient electron transport layer. Consequently, high photovoltage of 0.829 V is achieved with an efficiency of 9.4%, which is a record to our knowledge among TPSCs using SAMs as sole HTLs. While SAMs have been little used in TPSCs thus far, our holistic approach should catalyze their future advancements toward outperformance.



n lead-based perovskite solar cells (LPSCs), an inverted (p-i-n) architecture garners the spotlight due to recent progress in efficiency and stability. ¹⁻³ Specifically, the p-in LPSCs show the certified power conversion efficiency (PCE) of >25%^{1,2} and excellent operational stability under outdoor conditions. 1-3 Such recent progress primarily arises from the advent of self-assembled monolayers (SAMs) to serve as potent hole transport layers (HTLs).4 Since then, the fine engineering of perovskite film formation and the amelioration of top perovskite interfaces with electron transport layers (ETLs) have been accompanied. 1-3 Key features of SAMs such as lossless optoelectrical properties (i.e., high quasi-Fermi level splitting, negligible parasitic light absorption loss, etc.) along with interface passivation and facilitation of crystal growth could elicit additional increases in PCE. The elimination of dopants in SAMs could improve the stability of perovskite solar cells because the migration of dopants into perovskite layers is considered one factor that degrades devices. Besides, their high molecular tunability, ambient-air and low-temperature (${\lesssim}100~^{\circ}\text{C})$ processability, and ease of scalability via dipping make SAMs suitable for wide

Tin-based perovskite solar cells (TPSCs) are the embodiment of promising next-generation photovoltaics because they hold not only the fundamental merits of lead counterparts, such as high tunability, mechanical flexibility, light weight, and scalability, but also unique merits, including the absence of the toxic element of lead, smaller bandgap (~1.3–1.5 eV), and decent charge carrier mobility. Tight-performance TPSCs (with PCEs approaching 15%) utilize a p-i-n architecture,

where poly(3,4-ethylenedioxythiophene):poly(styrenesulfonate) (PEDOT:PSS) is almost universally employed as an HTL. The polar components exposed at the PEDOT:PSS surfaces can interact strongly via hydrogen bonding with perovskite precursors to promote tin perovskite crystallization and lamination. However, the hygroscopic nature of PEDOT:PSS could induce the formation of interface defects and the degradation of tin perovskites, likely through the breakage of axial Sn–I bonds by H₂O. 11

SAMs can become an ideal replacement for PEDOT:PSS in TPSCs despite a handful of reports. $^{12-15}$ The highest efficiency among TPSCs with SAMs as sole HTLs is 8.3% to date. 13 One reason for the inferior efficiency relative to the PEDOT:PSS devices comes from the open-circuit voltage ($V_{\rm oc}$) below 0.65 V, which is very low in considering a $V_{\rm oc}$ loss of >0.7 V for a $\gtrsim 1.4$ eV bandgap, $^{12-14}$ leaving significant room for improvement. $^{13-15}$ Usually in those devices, a two-step deposition method, where tin iodide and organic ammonium salts are sequentially deposited, is exploited for perovskite films with decent crystal quality and good lamination onto SAMs. 13 The principal downside of the two-step method stems from the imbalanced distribution of perovskite components across the

Received: January 15, 2024 Revised: February 17, 2024 Accepted: March 7, 2024



ACS Energy Letters http://pubs.acs.org/journal/aelccp Letter

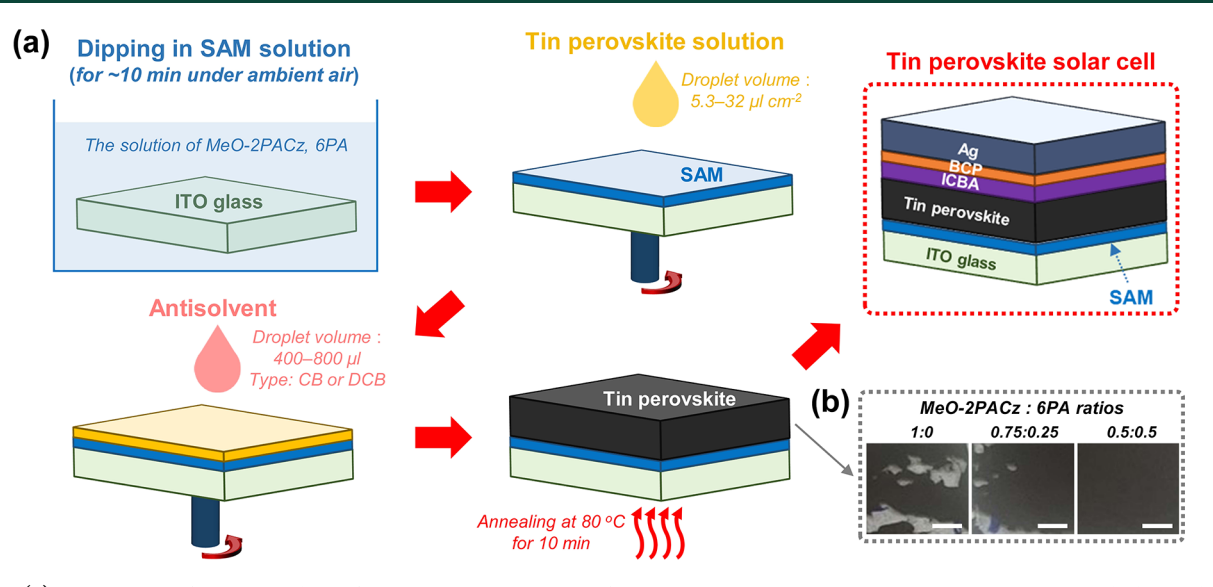


Figure 1. (a) Schematics of the procedures for making SAMs with different MeO-2PACz:6PA molar ratios on ITO-coated glass substrates and forming tin perovskite films atop SAM HTLs via an antisolvent-assisted one-step solution process. Further details are described in the Supporting Information. (b) Photographs of the resulting tin perovskite films on the SAMs at the different MeO-2PACz:6PA molar ratios (scale bar: 3 mm).

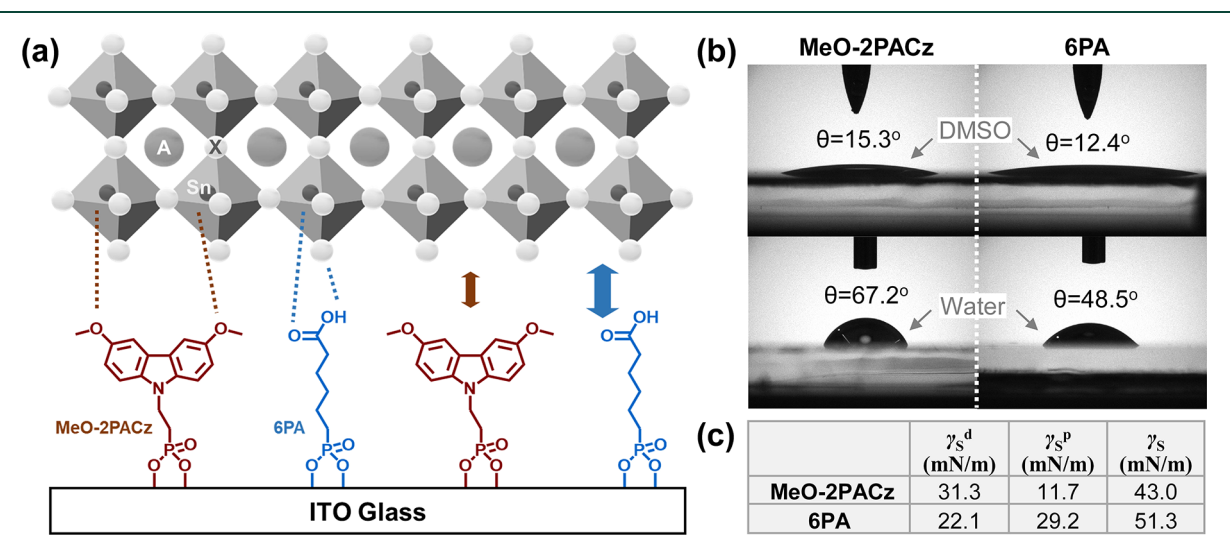


Figure 2. (a) Schematic illustration of the interaction between tin perovskite and different SAM molecules: MeO-2PACz and 6PA. In the perovskite crystal, A, X, and Sn stand for ammonium cations, halide anions, and divalent tin. (b) Contact angles of DMSO and water on SAMs of MeO-2PACz and 6PA on ITO-coated glass substrates. (c) Surface energies (γ_s) of the SAMs of MeO-2PACz and 6PA.

cross-section of the films. ¹⁶ Thus, it is likely that the top perovskite surface is enriched with electrically insulating organic salts to vary the energy level of the conduction band minimum (CBM) and hinder electron transport. This could pose a challenge in selecting efficient ETL materials. In contrast, an antisolvent-assisted one-step deposition method, which has been commonly used on PEDOT:PSS HTLs, ^{10,17} can avoid this issue and furthermore can be advantageous over forming tin perovskites of high quality, hence being promising for SAM-based TPSCs. Even though one relevant report has been recently published, the reported performance does not exceed that of the two-step method. ¹⁴ We thus posit that the one-step method has not yet been well-established for tin perovskites on SAM HTLs. ^{11,18}

In this work, we successfully demonstrate SAM-based TPSCs that exhibit a $V_{\rm oc}$ as high as 0.829 V and a PCE of 9.4%. Laminating tin perovskite films while attaining perovskite

crystals of demanding quality onto SAM HTLs is key, for which we construct a sticky SAM surface and discover the key parameters of the one-step method. In addition, we seek and leverage a high-performance ETL. Our approach is holistic, spanning the SAM HTL, tin perovskite, and ETL, as elaborated in the following.

Figure 1a shows an experimental procedure of the fabrication of a TPSC with a p-i-n architecture of ITO glass/SAM/tin perovskite/ICBA/BCP/Ag, where ITO, ICBA and BCP stand for indium tin oxide, indene-C₆₀ bisadduct, and bathocuproine, respectively. The three key components of the holistic approach are also illustrated in Figure 1a. First, to adjust the surface properties of SAMs, we choose two molecules, (2-(3,6-dimethoxy-9H-carbazol-9-yl)ethyl)-phosphonic acid (MeO-2PACz) and 6-phosphonohexanoic acid (6PA), to form an interactive mixed SAM with the phosphonic acids capable of strong binding onto an ITO

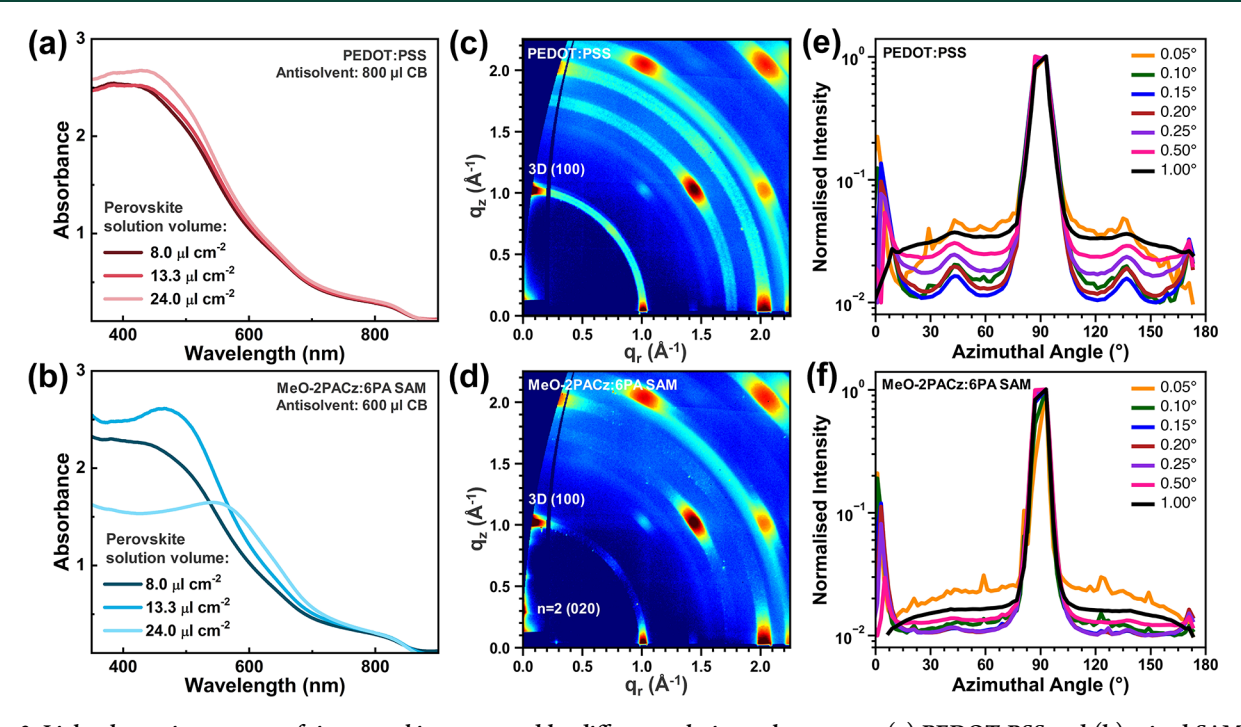


Figure 3. Light absorption spectra of tin perovskites prepared by different solution volumes onto (a) PEDOT:PSS and (b) mixed SAM at an equimolar ratio of MeO-2PACz to 6PA. (c-f) GIWAXS results of the tin perovskite films atop (c, e) PEDOT:PSS and (d, f) the mixed SAM formed with the optimal conditions of tin perovskite solution of 8 and 13.3 μ L cm⁻² for PEDOT:PSS and mixed SAM, respectively: (c, d) GIWAXS heat maps at the incidence angle of 0.20°; (e, f) azimuthal integration plots of the peaks between 0.95 and 1.05 Å⁻¹ at 0.05–1.00° grazing-incidence angles.

glass, 18 the methoxy group (-OCH3) and carboxylic acid group (-COOH) to interact with tin perovskites, 4,12 and the p-type carbazole group in MeO-2PACz to promote hole transfer. In particular, 6PA is essential for perovskite lamination for efficient hole transfer as well as light harvesting. 6PA and MeO-2PACz are subjected to negligible loss in light transmittance, particularly beyond the wavelength of 500 nm, compared to PEDOT:PSS (Figure S1). While spin-coating is often used for the deposition of SAMs, we use dipping to enhance compatibility with upscaling. Second, due to the difference in surface energy and chemistry of SAM HTLs and the commonly used PEDOT:PSS HTL, the condition of the antisolvent-assisted one-step process for tin perovskite films such as the volumes of precursor and antisolvent must be adjusted to ensure excellent coverage of tin perovskite solution and lamination and quality of the resulting perovskite film on SAMs. As shown in Figure 1b, the lower hydrophilicity of the terminal group of MeO-2PACz than the precursor solvent DMSO results in the delamination of the tin perovskite film. In contrast, a fully covered, uniform tin perovskite film is formed on the SAM with an equimolar ratio of MeO-2PACz to 6PA. Third, to enhance electron transport and increase $V_{\rm oc}$, we adopt ICBA as an ETL because ICBA can effectively passivate the perovskite top surface against Sn(IV) defects and is suitable for the uplifted CBM energy levels of the analogous tin perovskites. 5,10,19 The so-far developed SAM-based TPSCs use buckminsterfullerenes (namely, C₆₀) as an ETL, ¹²⁻¹⁴ resulting in low $V_{\rm oc}$ (<0.65 V) due to its inefficient surface passivation. Our preliminary results also show the same trend (Figure S2) with the C_{60} analogue and ICBA. The V_{oc} enhancement by ICBA is significant despite the heterogeneous top surfaces of tin perovskite films (Figure S3). The details of the aforementioned holistic approach are elaborated and discussed in the following paragraphs.

Introducing 6PA to form a MeO-2PACz:6PA mixed SAM can promote the interaction of tin perovskites with carboxylic acids via the OH···halide hydrogen bonds and C=O···Sn²⁺ coordination bonds²⁰ in addition to the C-O···Sn²⁺ coordination bonds²¹ from MeO-2PACz (Figure 2a). 6PA enables the hydrogen bonds that could suppress iodide vacancies and hence lower the trap-state density of tin perovskites. Moreover, 6PA also improves the wettability of DMSO, which is the sole solvent used for the tin perovskite solution in this work. The contact angles of DMSO and water on the SAM of pure 6PA are reduced compared to that on the SAM of pure MeO-2PACz (Figure 2b), indicating that 6PA is more hydrophilic and can improve the wettability of the DMSO-based tin perovskite solution. The surface energy (γ_s) was calculated using the Owens-Wendt-Kaelble equation: $\frac{\gamma_l(1+\cos\theta)}{2}=(\gamma_l^d\gamma_s^d)^{0.5}+(\gamma_l^p\gamma_s^p)^{0.5}, \text{ where } \gamma_s=\gamma_s^d+\gamma_s^p, \gamma_l \text{ and } \theta$ are the surface tension and contact angle, respectively, of DMSO or water, and γ^d and γ^p stand for the dispersion and polar components, respectively. The calculated values of γ_s^d , γ_s^p , and γ_s are tabulated in Figure 2c. For comparison, the contact angle and surface energy results for PEDOT:PSS are presented in Figure S4. The calculated γ_s is increased on the 6PA SAM due to a larger contribution of the polar component, which is about 2.5-fold greater compared to that of the MeO-2PACz SAM. The larger polar component, attributable to the stronger interaction of the SAM with tin perovskite solution, can create sufficient nucleation sites. Considering that nuclei could be sparse on HTLs of low surface energies and tin perovskites are known to undergo rapid crystal growth prior to completion of nucleation, 17,23 densifying the nuclei becomes crucial to the formation of perovskite crystals of demanding quality. In addition, it can promote heterogeneous crystallization for the lamination of perovskite films.

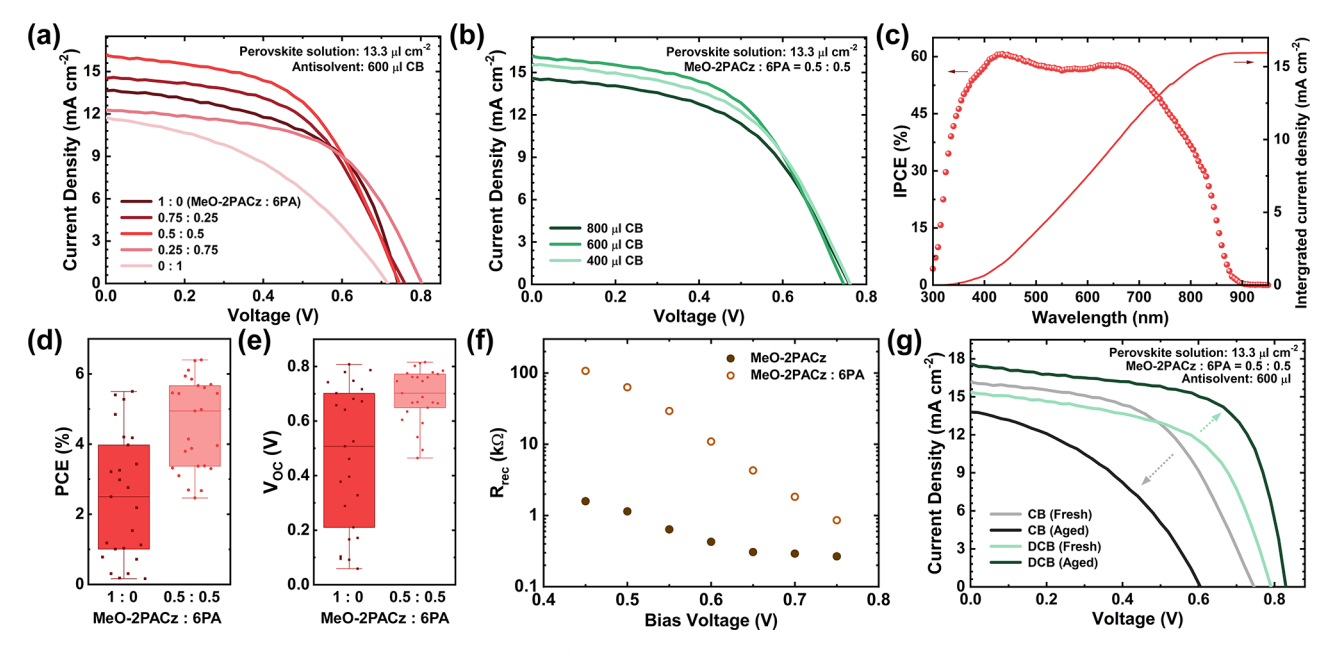


Figure 4. Representative J-V curves of the TPSCs with (a) various MeO-2PACz:6PA molar ratios and 600 μ L of CB antisolvent and (b) various CB volumes and an equimolar ratio of MeO-2PACz to 6PA. (c) IPCE spectrum and the integrated current density of the best TPSC in (b). (d, e) Histograms of PCE and $V_{\rm oc}$ of the SAM devices prepared with the 13.3 μ L cm⁻² perovskite solution and 600 μ L of CB antisolvent. (f) $R_{\rm rec}$ as a function of bias voltage, attained by impedance spectroscopy. (g) Effect of antisolvents of CB and DCB on J-V curves and their evolutions in a week.

Despite the advantages of mixed SAMs of MeO-2PACz:6PA, tin perovskite film formation conditions must be carefully adjusted using the polar solvent DMSO for tin perovskite solution and the nonpolar antisolvent chlorobenzene (CB). As we initially applied the same perovskite deposition condition for PEDOT:PSS (i.e., 8 µL cm⁻² 0.85 M tin perovskite solution and 800 μ L of CB antisolvent)²⁴ to SAMs of pure MeO-2PACz and an equimolar ratio of MeO-2PACz to 6PA, both led to local delamination of the tin perovskite films, which is more pronounced along the edges of the substrates. We posited that higher nuclei density could promote the lamination. We thus increased the solution concentration from 0.85 to 1.05 M. However, the short-circuit current (J_{sc}) is substantially sacrificed (Figure S5 and Table S1), which is attributable to the inefficient conversion to tin perovskite crystals. Instead, we turned our attention to the more pronounced delamination along the substrate edges. One reason for the edge delamination stems from partial dewetting of the perovskite solution before spin-coating due to lower surface energies of SAMs as compared to PEDOT:PSS; the details of spin-coating are described in the Supporting Information. To systematically understand and address this issue, we controlled the volume of perovskite solution in a wide range of 5.3-32.0 μ L cm⁻² while keeping the 0.85 M tin perovskite solution concentration and fixing the CB antisolvent volume to 800 μ L. The light absorption spectra of tin perovskite films formed on PEDOT:PSS show a trend of increased film thickness with rising solution volume from 8 to 24 μ L cm⁻² (Figure 3a). The tin perovskite films formed on the mixed SAM of MeO-2PACz:6PA show the same trend with the solution volume (Figure 3b). However, the light absorption in the wavelength range of >600 nm is attenuated more with the mixed SAM, revealing its higher sensitivity to the solution volume. Moreover, using the high solution volume $(24 \mu L \text{ cm}^{-2})$ for the mixed SAM gives rise to lowered light absorption in the wavelength range of <600 nm. We noticed

that the film color changed from dark brown (at the initial few seconds upon antisolvent dripping) to transparent (during the remaining spin-coating and before annealing) and hazy black (during the subsequent annealing), which is due to the insufficient volume of antisolvent when the larger solution volume (24 μ L cm⁻²) was used. We need to note that increasing the antisolvent volume up to 1000 µL did not resolve this issue, due likely to the rapid crystallization from the top. Further discussion on the critical role of solution volume in forming tin perovskites of desired quality is provided specifically in relation to the antisolvent volume in the Supporting Information. The effects of the solution volume on the SAM are assessed in TPSCs whose representative J-Vcurves and photovoltaic parameters are presented in Figure S6 and Table S2. The results show that the solution volume of 13.3 μ L cm⁻² yielded the best PCE of 4.1%.

The tin perovskite films formed with the optimal volumes of tin perovskite solution and antisolvent on PEDOT:PSS and the mixed SAM with an equimolar ratio of MeO-2PACz to 6PA were investigated in crystallographic properties, aided by grazing-incidence wide-angle X-ray scattering (GIWAXS). The tin perovskite film on PEDOT:PSS is characterized by the presence of Debye-Scherrer rings corresponding to the (100), (110), (111), and (200) planes of cubic 3D tin perovskite (Figure 3c), suggesting a certain degree of randomness in the crystal orientation. This randomness in crystal orientation is persistent across multiple grazing-incidence angles (Figure S7), meaning that it is across the depth profile. In contrast, the tin perovskite film on the mixed SAM is characterized by pronounced Bragg spots (Figure 3d), which are present throughout the entire film cross section (Figure S8). This imparts that more oriented 3D crystal structures are formed on the mixed SAM. In particular, the (100) plane peak is more concentrated along the q_z axis for the film on the mixed SAM than that on PEDOT:PSS, suggesting a greater degree of vertical orientation. Moreover, a majority of crystallites formed

on the mixed SAM are perpendicularly oriented to the substrate, as opposed to those on PEDOT:PSS, as examined by the azimuthal integration of the (100) plane peak across different profiling depths (Figure 3e,f). The tin perovskite film formed on the mixed SAM also displays the presence of a 2D phase with n = 2 throughout the entire film cross section, which is almost absent on PEDOT:PSS (Figure S9). While more discussions are made in the Supporting Information, the aforementioned GIWAXS results could originate from the template effect at the interface of the mixed SAM and tin perovskite film. The template effect would be a result of the reduced nuclei density on the SAM. Meanwhile, as smaller (8 $\mu L \text{ cm}^{-2}$) and larger (24 $\mu L \text{ cm}^{-2}$) volumes of the perovskite solutions are used on the mixed SAM, the perovskite films show the increased feature of Debye-Scherrer rings and two small peaks at the azimuthal angles of 45 and 135° (Figure S10), indicating more randomness of crystal orientations. Overall, the GIWAXS results confirm that the tin perovskite film formed with the optimal precursor solution volume on the SAM possesses crystallographic properties that are desirable for photovoltaic applications.

In Figure 4, the TPSC results are presented. The J-V curves in Figures 4a and S11 and their photovoltaic parameters in Table S3 result from the mixed SAMs of MeO-2PACz:6PA with various molar ratios and CB antisolvent volumes but with the fixed perovskite solution volume (13.3 μ L cm⁻²). Above all, all $V_{\rm oc}$ values are in the range of 0.668-0.802 V, exceeding the highest $V_{\rm oc}$ (~0.65 V) reported for TPSCs on pure SAM HTLs. In addition, it is verified that the equimolar ratio of the mixed SAM is optimal because it gives the highest $J_{\rm sc}$. While the perovskite is laminated with partial coverage onto the substrate at MeO-2PACz-dominant ratios (1:0 and 0.75:0.25), the hole transfer is appreciably limited at 6PAdominant ratios (0.25:0.75 and 0:1) due to the decreased ptype character. The interplay of these two parameters leads to the most efficient light harvesting and hole transfer at the equimolar ratio, contributing to the highest J_{sc} . At the equimolar ratio of the mixed SAM, the best efficiency was enabled by the 600 μ L of CB antisolvent (Figure 4b), benefiting from the highest J_{sc} and fill factor (FF) in spite of the lowest V_{oc} . Figure 4c shows an incident-photon-to-current conversion efficiency (IPCE) spectrum of the best device in Figure 4b. The integrated current density in the IPCE spectrum matches well with that in the I-V curve. Besides, small J-V hysteresis behavior and enhanced stabilized power output are obtained, as shown in Figure S12a,b.

Statistical histograms of the photovoltaic performance of the TPSCs prepared on the SAM HTLs of pure MeO-2PACz and an equimolar ratio of MeO-2PACz to 6PA are provided in Figures 4d,e and S13. Desirably, the higher mean values and smaller spreads of photovoltaic parameters are obtained with the mixed SAM. These results arise from the enhanced lamination of tin perovskites to promote hole transfer while suppressing hole recombination with uniformity across the entire film cross section. This is further corroborated by the results from the impedance spectroscopy studies. Figure 4f shows the recombination resistance (R_{rec}) , extracted from the raw data fitting using an equivalent circuit (Figure S14), as a function of the bias voltage. Overall, the TPSC with the mixed SAM exhibits about 30-fold higher R_{rec} on average than that with the pure MeO-2PACz SAM, indicating greatly suppressed recombination. The R_{rec} of the mixed SAM-based TPSCs is >10-fold greater than that of the PEDOT:PSS-based TPSCs

with the same perovskite composition despite the competitive PCEs between them. ²⁴ Meanwhile, the defect density of the tin perovskite film on the mixed SAM was calculated to be 8.61 × 10^{15} cm⁻³ by a Mott–Schottky plot (Figure S15), which is approximately 5-fold lower than that on PEDOT:PSS (4.41 × 10^{16} cm⁻³). ²⁴ Taken together, the higher $R_{\rm rec}$ and lower defect density on the mixed SAM compared with PEDOT:PSS align with the excellent perovskite lamination and the GIWAXS results exhibiting the oriented 3D perovskite crystallites and the 2D phase throughout the cross section of the entire films. Similar results by SAMs have been reported for lead PSCs. ^{1,4}

In addition to the antisolvent volume, the antisolvent type should play a key role for the TPSC performance, as distinct chemiphysical properties from PEDOT:PSS are brought by the mixed SAM. Hence, we replaced the antisolvent CB with 1,2dichlorobenzene (DCB). Like CB, DCB is miscible with DMSO with ease. Importantly, the boiling point of DCB is higher than that of CB and closer to that of DMSO, which during the annealing leads to the suppression of bubble formation and thus voids²⁵ as well as slower evaporation for better control of tin perovskite crystallization atop of SAMs. Indeed, the TPSCs fabricated with the DCB antisolvent exhibit an increased initial PCE from 6.4% to 6.9% on account of the rises in V_{oc} and FF (Figure 4g); full photovoltaic parameters are summarized in Table S4. Importantly, the PCE further increased to 9.4% after 1 week of storage in a N2-filled glovebox in the dark on account of rises in all photovoltaic parameters, V_{oc} (0.791 to 0.829 V), J_{sc} (15.3 to 17.6 mA cm⁻²), and FF (57.3 to 64.5%). In striking contrast, the TPSCs fabricated with the CB antisolvent degraded with lowered photovoltaic parameters, $V_{\rm oc}$ (0.746 to 0.604 V), $J_{\rm sc}$ (16.1 to 13.8 mA cm⁻²), and FF (53.2 to 39.8%). To the best of our knowledge, the attained PCE and $V_{\rm oc}$ are the highest among TPSCs using SAMs as sole HTLs. The analogous beneficial effect driven by the high-boiling-point antisolvent was reported previously for TPSCs. 26 The dramatic enhancement of the PCE by DCB might be ascribed to the stabilized SAM/ perovskite interface. However, longer storage for 2 weeks did not lead to the same enhancement (Figure S16). While tin perovskites are vulnerable to their surroundings, future research on understanding the longer storage effect should proceed in terms of the stability of the tin perovskites.

To summarize, we successfully demonstrate high opencircuit voltage and power conversion efficiency of tin perovskite solar cells using a hole-transporting self-assembled monolayer. A holistic approach, including developing two different molecules in the self-assembled monolayer, controlling the fundamental perovskite deposition parameters, and leveraging an efficient electron transport layer, is key to the success. The approach reported herein is promising and offers a cornerstone toward taking full advantage of self-assembled monolayers for tin perovskite solar cells.

ASSOCIATED CONTENT

Supporting Information

The Supporting Information is available free of charge at https://pubs.acs.org/doi/10.1021/acsenergylett.4c00155.

Experimental section, current–voltage characteristics, contact angles, surface energy table, scanning electron microscope images, Mott–Schottky plot, light absorption spectra, impedance spectra, and GIWAXS results (PDF)

AUTHOR INFORMATION

Corresponding Author

Qiuming Yu — Robert Frederick Smith School of Chemical and Biomolecular Engineering, Cornell University, Ithaca, New York 14853, United States; oorcid.org/0000-0002-2401-4664; Email: qy10@cornell.edu

Authors

Donghoon Song — Robert Frederick Smith School of Chemical and Biomolecular Engineering, Cornell University, Ithaca, New York 14853, United States; orcid.org/0000-0003-0914-1507

Shripathi Ramakrishnan — Robert Frederick Smith School of Chemical and Biomolecular Engineering, Cornell University, Ithaca, New York 14853, United States

Yugang Zhang — Center for Functional Nanomaterials, Brookhaven National Laboratory, Upton, New York 11973-5000, United States

Complete contact information is available at: https://pubs.acs.org/10.1021/acsenergylett.4c00155

Author Contributions

The manuscript was written through contributions of all authors. All of the authors approved the final version of the manuscript.

Notes

The authors declare no competing financial interest.

ACKNOWLEDGMENTS

We acknowledge the financial support from the National Science Foundation (NSF) (ECCS-2054942 and EPM-2114350). This work made use of the Cornell Center for Materials Research Shared Facilities which are supported through the NSF MRSEC Program (DMR-1719875) and the GIWAXS from the CMS beamline (11-BM) of the National Synchrotron Light Source II supported by the U.S. DOE Office of Science Facilities at Brookhaven National Laboratory under Contract No. DE-SC0012704. We thank Yuanze Xu for the contact angle measurements.

■ REFERENCES

- (1) Li, Z.; Sun, X.; Zheng, X.; Li, B.; Gao, D.; Zhang, S.; Wu, X.; Li, S.; Gong, J.; Luther, J. M.; Li, Z.; Zhu, Z. Stabilized Hole-Selective Layer for High-Performance Inverted p-i-n Perovskite Solar Cells. *Science* **2023**, 382 (6668), 284–289.
- (2) Liu, C.; Yang, Y.; Chen, H.; Xu, J.; Liu, A.; Bati, A. S. R.; Zhu, H.; Grater, L.; Hadke, S. S.; Huang, C.; Sangwan, V. K.; Cai, T.; Shin, D.; Chen, L. X.; Hersam, M. C.; Mirkin, C. A.; Chen, B.; Kanatzidis, M. G.; Sargent, E. H. Bimolecularly Passivated Interface Enables Efficient and Stable Inverted Perovskite Solar Cells. *Science* **2023**, 382 (6672), 810–815.
- (3) Li, G.; Su, Z.; Canil, L.; Hughes, D.; Aldamasy, M. H.; Dagar, J.; Trofimov, S.; Wang, L.; Zuo, W.; Jerónimo-Rendon, J. J.; Byranvand, M. M.; Wang, C.; Zhu, R.; Zhang, Z.; Yang, F.; Nasti, G.; Naydenov, B.; Tsoi, W. C.; Li, Z.; Gao, X.; Wang, Z.; Jia, Y.; Unger, E.; Saliba, M.; Li, M.; Abate, A. Highly Efficient P-i-n Perovskite Solar Cells That Endure Temperature Variations. *Science* **2023**, *379* (6630), 399–403.
- (4) Al-Ashouri, A.; Magomedov, A.; Roß, M.; Jošt, M.; Talaikis, M.; Chistiakova, G.; Bertram, T.; Márquez, J. A.; Köhnen, E.; Kasparavičius, E.; Levcenco, S.; Gil-Escrig, L.; Hages, C. J.; Schlatmann, R.; Rech, B.; Malinauskas, T.; Unold, T.; Kaufmann, C. A.; Korte, L.; Niaura, G.; Getautis, V.; Albrecht, S. Conformal Monolayer Contacts with Lossless Interfaces for Perovskite Single

- Junction and Monolithic Tandem Solar Cells. Energy Environ. Sci. 2019, 12 (11), 3356–3369.
- (5) Pitaro, M.; Tekelenburg, E. K.; Shao, S.; Loi, M. A. Tin Halide Perovskites: From Fundamental Properties to Solar Cells. *Adv. Mater.* **2022**, *34* (1), 2105844.
- (6) Ke, W.; Stoumpos, C. C.; Kanatzidis, M. G. Unleaded" Perovskites: Status Quo and Future Prospects of Tin-Based Perovskite Solar Cells. *Adv. Mater.* **2019**, *31* (47), 1803230.
- (7) Wu, T.; Liu, X.; Luo, X.; Lin, X.; Cui, D.; Wang, Y.; Segawa, H.; Zhang, Y.; Han, L. Lead-Free Tin Perovskite Solar Cells. *Joule* **2021**, 5 (4), 863–886.
- (8) Yu, B.-B.; Chen, Z.; Zhu, Y.; Wang, Y.; Han, B.; Chen, G.; Zhang, X.; Du, Z.; He, Z. Heterogeneous 2D/3D Tin-Halides Perovskite Solar Cells with Certified Conversion Efficiency Breaking 14%. *Adv. Mater.* **2021**, 33 (36), 2102055.
- (9) Jiang, X.; Li, H.; Zhou, Q.; Wei, Q.; Wei, M.; Jiang, L.; Wang, Z.; Peng, Z.; Wang, F.; Zang, Z.; Xu, K.; Hou, Y.; Teale, S.; Zhou, W.; Si, R.; Gao, X.; Sargent, E. H.; Ning, Z. One-Step Synthesis of SnI₂· (DMSO)_x Adducts for High-Performance Tin Perovskite Solar Cells. *J. Am. Chem. Soc.* **2021**, *143* (29), 10970–10976.
- (10) Song, D.; Ramakrishnan, S.; Xu, Y.; Yu, Q. Designing Effective Hole Transport Layers in Tin Perovskite Solar Cells. *ACS Energy Lett.* **2023**, 8 (10), 4162–4172.
- (11) Kaiser, W.; Ricciarelli, D.; Mosconi, E.; Alothman, A. A.; Ambrosio, F.; De Angelis, F. Stability of Tin- versus Lead-Halide Perovskites: Ab Initio Molecular Dynamics Simulations of Perovskite/Water Interfaces. *J. Phys. Chem. Lett.* **2022**, *13* (10), 2321–2329.
- (12) Song, D.; Narra, S.; Li, M.-Y.; Lin, J.-S.; Diau, E. W.-G. Interfacial Engineering with a Hole-Selective Self-Assembled Monolayer for Tin Perovskite Solar Cells via a Two-Step Fabrication. *ACS Energy Lett.* **2021**, *6* (12), 4179–4186.
- (13) Afraj, S. N.; Kuan, C.-H.; Lin, J.-S.; Ni, J.-S.; Velusamy, A.; Chen, M.-C.; Diau, E. W.-G. Quinoxaline-Based X-Shaped Sensitizers as Self-Assembled Monolayer for Tin Perovskite Solar Cells. *Adv. Funct. Mater.* **2023**, 33 (17), 2213939.
- (14) Aktas, E.; Poli, I.; Ponti, C.; Li, G.; Olivati, A.; Di Girolamo, D.; Alharthi, F. A.; Li, M.; Palomares, E.; Petrozza, A.; Abate, A. One-Step Solution Deposition of Tin-Perovskite onto a Self-Assembled Monolayer with a DMSO-Free Solvent System. *ACS Energy Lett.* **2023**, 8 (12), 5170–5174.
- (15) Chen, M.; Kapil, G.; Wang, L.; Razey Sahamir, S.; Baranwal, A. K.; Nishimura, K.; Sanehira, Y.; Zhang, Z.; Akmal Kamarudin, M.; Shen, Q.; Hayase, S. High Performance Wide Bandgap Lead-Free Perovskite Solar Cells by Monolayer Engineering. *Chem. Eng. J.* **2022**, 436, 135196.
- (16) Yang, W. S.; Noh, J. H.; Jeon, N. J.; Kim, Y. C.; Ryu, S.; Seo, J.; Seok, S. I. High-Performance Photovoltaic Perovskite Layers Fabricated through Intramolecular Exchange. *Science* **2015**, 348 (6240), 1234–1237.
- (17) Dong, H.; Ran, C.; Gao, W.; Sun, N.; Liu, X.; Xia, Y.; Chen, Y.; Huang, W. Crystallization Dynamics of Sn-Based Perovskite Thin Films: Toward Efficient and Stable Photovoltaic Devices. *Adv. Energy Mater.* **2022**, *12* (1), 2102213.
- (18) Hotchkiss, P. J.; Jones, S. C.; Paniagua, S. A.; Sharma, A.; Kippelen, B.; Armstrong, N. R.; Marder, S. R. The Modification of Indium Tin Oxide with Phosphonic Acids: Mechanism of Binding, Tuning of Surface Properties, and Potential for Use in Organic Electronic Applications. *Acc. Chem. Res.* **2012**, 45 (3), 337–346.
- (19) Jiang, X.; Wang, F.; Wei, Q.; Li, H.; Shang, Y.; Zhou, W.; Wang, C.; Cheng, P.; Chen, Q.; Chen, L.; Ning, Z. Ultra-High Open-Circuit Voltage of Tin Perovskite Solar Cells via an Electron Transporting Layer Design. *Nat. Commun.* **2020**, *11* (1), 1245.
- (20) Hu, F.; Chen, C.-H.; Lou, Y.-H.; Teng, T.-Y.; Shi, Y.-R.; Xia, Y.; Wang, K.-L.; Chen, J.; Wang, Z.-K.; Liao, L.-S. A Vertical Antioxidant Strategy for High Performance Wide Band Gap Tin Perovskite Photovoltaics. *J. Mater. Chem. A* **2023**, *11* (9), 4579–4586.
- (21) Cho, S.; Pandey, P.; Yoon, S.; Ryu, J.; Lee, D.-G.; Shen, Q.; Hayase, S.; Song, H.; Choi, H.; Ahn, H.; Oh, C.-M.; Hwang, I.-W.; Cho, J. S.; Kang, D.-W. Anchoring Self-Assembled Monolayer at

- Perovskite/Hole Collector Interface for Wide Bandgap Sn-Based Solar Cells with a Record Efficiency over 12%. *Surf. Interfaces* **2023**, 42, 103478.
- (22) Du, Y.; Xu, J.; Sakizadeh, J. D.; Weiblen, D. G.; McCormick, A. V.; Francis, L. F. Modulus- and Surface-Energy-Tunable Thiol-Ene for UV Micromolding of Coatings. ACS Appl. Mater. Interfaces 2017, 9 (29), 24976–24986.
- (23) Bi, C.; Wang, Q.; Shao, Y.; Yuan, Y.; Xiao, Z.; Huang, J. Non-Wetting Surface-Driven High-Aspect-Ratio Crystalline Grain Growth for Efficient Hybrid Perovskite Solar Cells. *Nat. Commun.* **2015**, *6* (1), 7747
- (24) Song, D.; Li, H.; Xu, Y.; Yu, Q. Amplifying Hole Extraction Characteristics of PEDOT:PSS via Post-Treatment with Aromatic Diammonium Acetates for Tin Perovskite Solar Cells. *ACS Energy Lett.* **2023**, 8 (8), 3280–3287.
- (25) Sangale, S. S.; Kwon, S.-N.; Patil, P.; Lee, H.-J.; Na, S.-I. Locally Supersaturated Inks for a Slot-Die Process to Enable Highly Efficient and Robust Perovskite Solar Cells. *Adv. Energy Mater.* **2023**, *13* (33), 2300537.
- (26) Liu, X.; Yan, K.; Tan, D.; Liang, X.; Zhang, H.; Huang, W. Solvent Engineering Improves Efficiency of Lead-Free Tin-Based Hybrid Perovskite Solar Cells beyond 9%. ACS Energy Lett. 2018, 3 (11), 2701–2707.